JOURNAL OF SCIENCE
SAKARYA UNIVERSITY

Sakarya University Journal of Science

ISSN 1301-4048 | e-ISSN 2147-835X | Period Bimonthly | Founded: 1997 | Publisher Sakarya University | http://www.saujs.sakarya.edu.tr/

Title: Heat Transfer Analysis Of Different Thermal Oils İn Parabolic Trough Solar Collectors With Longitudinal Sinusoidal İnternal Fin

Authors: Burak Kurşun
Recieved: 2018-12-07 17:47:51

Accepted: 2019-04-15 14:21:27

Article Type: Research Article
Volume: 23
Issue: 5
Month: October
Year: 2019
Pages: 848-858

How to cite
Burak Kurşun; (2019), Heat Transfer Analysis Of Different Thermal Oils İn Parabolic Trough Solar Collectors With Longitudinal Sinusoidal İnternal Fin. Sakarya University Journal of Science, 23(5), 848-858, DOI: 10.16984/saufenbilder.493707
Access link
http://www.saujs.sakarya.edu.tr/issue/44066/493707

Sakarya University Journal of Science 23(5), 848-858, 2019

Heat transfer analysis of different thermal oils in parabolic trough solar collectors with longitudinal sinusoidal internal fin

Burak Kurşun*[1]

Abstract

Parabolic trough solar collectors (PTSC) plays an important role in the heating of fluids and in the generation of electricity . In this study, heat transfer and temperature distribution analysis was carried out for the use of internal longitudinal fins with different geometries in a parabolic trough solar collector. Numerical analyzes were carried out for different Reynolds (Re) numbers ($2x10^4$-8 $x10^4$) at steady-state conditions and three different thermal oils were used as heat transfer fluid (HTF). The use of the internal fin with sinusoidal lateral surface for all types of thermal oil increased the heat transfer and made the temperature distribution in the fluid more uniform. The highest thermal enhancement factor was occurred for Syltherm 800 oil and sinusoidal fin geometry. With the use of Syltherm 800 oil, the thermal enhancement factor (ψ) increased by 40% and 44% respectively according to the Therminol VP1 and D12 oil type for the case with sinusoidal fin.

Keywords: Longitudinal fin, Parabolic trough, Sinusoidal fin, Thermal oil

1. INTRODUCTION

Renewable energy sources are nowadays widely used as an alternative to energy sources that create air pollution and negatively affect ecological life. Renewable energy can be classified as energies of solar, wind, hydrogen and biomass. Concentrated solar power (CSP) systems play an important role in the heating of fluids and in the generation of electricity. This study focused on parabolic trough solar collectors (PTSC) used in medium temperature (100-400°C) applications [2].

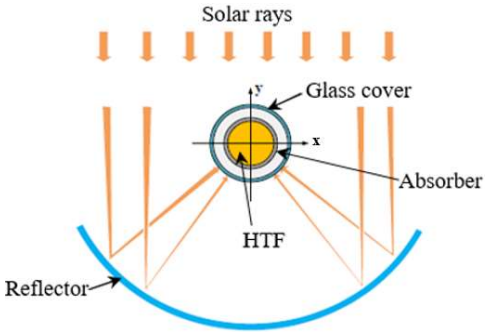

Figure 1. Parabolic trough collector[1]

PTSCs are composed of a parabolic reflector, glass cover and a circular shaped absorber through which the fluid passes. The sun rays are focused on the absorber by reflectors and the fluid in the absorber is heated (Figure 1). There are many experimental and numerical studies to increase the thermal performance of PTSCs.

* Corresponding Author: burak.kursun@amasya.edu.tr

[1] Amasya University, Mechanical Engineering, Amasya, Turkey, ORCID: 0000-0001-5878-3894

Inserts for absorber have been widely applied in these studies [2]. Cheng et al. investigated the effect of an absorber with unilateral milt-longitudinal vortex generators on thermal performance, numerically [3]. Numerical study showed that the vortex generators increased heat transfer by 2.23-13.62%. The use of the twisted tape insert with different nanofluids in the absorber was presented by Waghole et al. [4]. Experimental study revealed that the heat transfer and the pressure loss increase by 1.5-2.10 times and 1-1.75 times respectively. In the study carried out by Kumar and Reddy, perforated disc usage in the absorber was investigated, numerically [5]. For the optimal configuration of the porous disc, it was observed that the heat transfer and the pressure loss increased by 221 watt and 13.5%, respectively. The effect of inserting metal foam in the absorber on the heat transfer was analysed by Wang et al. [6]. The geometry and the porosity of the metal foam were investigated. It was reported that the increase in the Nusselt number (Nu) and the friction coefficient were 10-20 times and 400-700 times, respectively. Investigating of the use of a louvered twisted-tape and the typical plain twisted-tape inserts in the absorber performed by Ghadirijafarbeigloo et al. [7]. For the fully developed turbulent conditions, the louvered twisted-tape inserts significantly increased the heat transfer and pressure loss compared to typical plain twisted-tape inserts. Jaramillo et al. investigated thermal performance by using twisted-tape inserts in a parabolic trough collector for low enthalpy processes [8]. It was revealed that the higher increase in the heat transfer occurred for the low twist ratio and the Reynolds number (Re) values. For a tubular absorber, using of the dimples, protrusions and internal helical fins on the heat transfer were determined by Huang et al. [9]. The highest enhancement in the Nu and friction coefficient by 44-64% and 56-77%, respectively, by using a dimpled tube. In the presented study by Gong et al., the heat transfer enhancement was provided by using an absorber with pin fin inserts [10]. It was reported, the Nu and overall heat transfer performance factor were increased by 9% and 12% respectively for the pin fin usage. Bellos et al. presented a study including the effect of the internal fin with different length and thickness on the thermal performance for the parabolic trough collector [11]. Numerical study showed that increase in the fin thickness and length increased the pressure loss and heat transfer.

It is clear from the literature that the use of inserts for absorber tube increases the heat transfer. Although there are many experimental and numerical studies for inserts with different geometries, there are few studies on the effect of lateral surface geometry of the inserts on heat transfer. In this study, thermal performance analysis was carried out for the use of internal longitudinal fins with sinusoidal lateral surfaces in a parabolic trough solar collector. Sinusoidal geometry are widely used in compact heat exchangers due to the higher thermal performance [12-14]. Thus, sinusoidal geometry was preferred for the numerical analyses. The main aim of the study is to investigate the effect of different types of thermal oil on heat transfer and pressure drop for sinusoidal internal finned absorber. For this purpose, three different types of thermal oil: Syltherm 800, Therminol D12 and Therminol VP1 were used. Numerical analyzes were performed for the conditions with flat fin, sinusoidal fin and without fin and the findings obtained were compared with each other.

2. PHYSICAL MODEL

Absorber geometry used for numerical analysis was given in Figure 2. Figure 2a and 2b represent the flat and the sinusoidal fin geometries, respectively. In Figure 2c, the amplitude value (a) of sinusoidal geometry is a=6mm, periodic length (p) is p=10mm and thickness (t) is t=5mm. The fin heights (H) are H=5mm for all conditions.

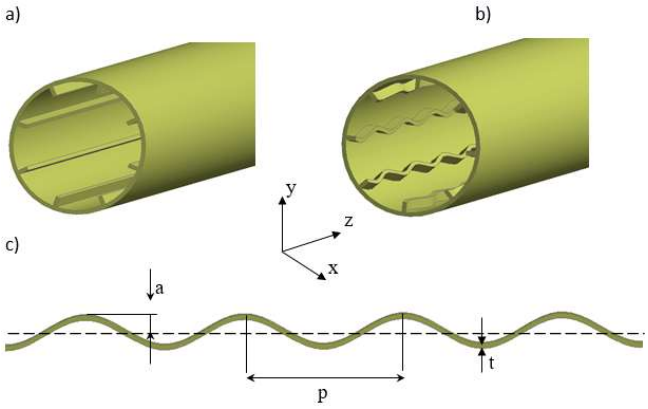

Figure 2. LS-2 absorber and fin geometry, a) flat fin, b)sinusoidal fin, c)sinusoidal geometry

The absorber geometry was modeled according to the LS-2 type receiver dimensions [15] and the absorber material was 316L steel [16]. The values of the absorber dimensions and the thermal properties of the absorber material are given in Table 1. The inlet

temperature of the thermal oils (T_{in}) to the absorber was determined by taking into account the thermal properties such as boiling and autoignition temperature (T_{in}=400 K). The thermal properties of Syltherm 800, Therminol D12 and VP1 oils for 400 K temperature were taken from References [11] and [25] respectively (Table 2). Because the absorbing geometry was symmetrical with respect to the y-z plane, half of the absorber was modeled for numerical analysis.

Table 1. Dimension values of LS-2 absorber and thermal properties of absorber material

Absorber		316L steel	
D_i(m)	0.066	λ(W/m.K)	24.92
D_0(m)	0.070	ρ(kg/m^3)	8030
L(m)	7.8	C_p(J/kg.K)	502.48

Table 2. Thermal properties of oils (T=400K)

Oil type	λ(W/m.K)	ρ(kg/m^3)	C_p(J/kg.K)	μ(Pa.s)
Slyth800	0.1149	840.3	1791	0.00222
VP1	0.1243	977	1850	0.000731
D12	0.0917	681	2520	0.000356

3. MATHEMATICAL MODEL

In the numerical analysis, it was assumed that the fluids were incompressible and their thermal properties were constant. The analyzes were performed under steady-state and turbulent flow conditions. The three-dimensional governing equations are given below. Equations 1, 2 and 3 are the conservation of mass, momentum and energy, respectively.

$$\frac{\partial}{\partial x_i}(\rho u_i) = 0 \tag{1}$$

$$\frac{\partial}{\partial x_j}(\rho u_i u_j) = -\frac{\partial P}{\partial x_i} + \frac{\partial}{\partial x_j}\left[\mu\left(\frac{\partial u_i}{\partial x_j} + \frac{\partial u_j}{\partial x_i}\right) - \frac{2}{3}\mu\frac{\partial u_i}{\partial x_i}\delta_{ij} - \rho\overline{u_i{}'u_j{}'}\right] \tag{2}$$

$$\frac{\partial}{\partial x_j}(\rho u_j C_p T) = \frac{\partial}{\partial x_j}\left(\lambda\frac{\partial T}{\partial x_j} + \frac{\mu_t}{\sigma_{h,t}}\frac{\partial (C_p T)}{\partial x_j}\right) + u_j\frac{\partial P}{\partial x_j} + \left[\mu\left(\frac{\partial u_i}{\partial x_j} + \frac{\partial u_j}{\partial x_i}\right) - \frac{2}{3}\mu\frac{\partial u_i}{\partial x_i}\delta_{ij} - \rho\overline{u_i{}'u_j{}'}\right]\frac{\partial u_i}{\partial x_j} \tag{3}$$

Where, u_i and u_j are the time-averaged velocity components in the i and j directions, $\rho\overline{u_i{}'u_j{}'}$ are the Reynolds stresses, P is the time-averaged pressure, T is the time-averaged temperature, λ is the fluid thermal conductivity, ρ is the density, μ_t is the turbulent viscosity and $\sigma_{h,t}$ is the turbulent Prandtl number for energy. The Reynolds stresses can be expressed by the following equation depending on the Boussinesq hypothesis to include velocity gradients [19],

$$\rho\overline{u_i{}'u_j{}'} = \mu\left(\frac{\partial u_i}{\partial x_j} + \frac{\partial u_j}{\partial x_i}\right) - \frac{2}{3}\mu\left(\rho k + \mu_t\frac{\partial u_k}{\partial x_k}\right)\delta_{ij} \tag{4}$$

Where δ_{ij} is the linear deformation rate of a fluid element, k is the turbulent kinetic energy per unit mass. δ_{ij} and k are given by Equations 5 and 6,

$$\delta_{ij} = \frac{1}{2}\left(\frac{\partial u_i}{\partial x_j} + \frac{\partial u_j}{\partial x_i}\right) \tag{5}$$

$$k = \frac{1}{2}\left(\overline{u'^2} + \overline{v'^2} + \overline{w'^2}\right) \tag{6}$$

k-ε model is widely used in flow calculations [19,20]. Realisable k-ε model was selected in the present study. In the Realisable k-ε model, the two additional equations used for the transport of turbulence kinetic energy (k) and turbulent dissipation rates (ε)are given below,

k equation:

$$\frac{\partial}{\partial x_j}(\rho k u_j) = \frac{\partial}{\partial x_i}\mu\left[\left(\mu + \frac{\mu_t}{\sigma_k}\right)\frac{\partial k}{\partial x_j}\right] + G_k - \rho\varepsilon \tag{7}$$

ε equation:

$$\frac{\partial}{\partial x_j}(\rho\varepsilon u_j) = \frac{\partial}{\partial x_i}\mu\left[\left(\mu + \frac{\mu_t}{\sigma_\varepsilon}\right)\frac{\partial \varepsilon}{\partial x_j}\right] + \rho C_1 S\varepsilon - \rho C_2\frac{\varepsilon^2}{k+\sqrt{\nu\varepsilon}} \tag{8}$$

Where σ_k and σ_ε are the turbulent Prandtl number for k and ε, respectively. G_k is the production of turbulent kinetic energy and calculated by Equation 9,

$$G_k = -\rho\overline{u_i{}'u_j{}'}\frac{\partial u_j}{\partial x_i} \tag{9}$$

When the G_k equation is evaluated together with the Equation 4, the following equation can be written,

$$G_k = \mu_t S^2 \tag{10}$$

Turbulent viscosity is given by Equation 11,

$$\mu_t = \rho C_\mu\frac{k^2}{\varepsilon} \tag{11}$$

Constants used in the Realisable k-ε model are given below,

$C_1 = max\left[0.43, \frac{\eta}{\eta+5}\right], \eta = S\frac{k}{\varepsilon},\ S \equiv \sqrt{S_{ij}S_{ij}},\ C_2 = 1.9,\ \sigma_k = 1,\ \sigma_\varepsilon = 1.2$

C_μ is a function of the mean strain and rotation rates, the angular velocity, and the turbulence fields. Calculation of C_μ function is given in Reference [19].

3.1. Boundary Conditions

The uniform velocity distribution was accepted at the inlet of the absorber and the inlet velocity values were assigned in the z-axis direction depending on the variable Reynolds numbers (Re). At the absorber outlet, the pressure was taken equal to the gauge pressure value (Pressure outlet condition). The boundary conditions at the inlet and outlet of the channel for the symmetric model were expressed by Equations 12 and 13 respectively,

$$u = v = 0,\ w = w_{in},\ T = T_{in},\ 90^\circ \le \theta \le 270^\circ \quad (12)$$

$$P_{out} = P_{gage} = 0 \qquad 90^\circ \le \theta \le 270^\circ \quad (13)$$

In parabolic trough collectors, a non-uniform heat flux distribution occurs on the outer surface of the absorber due to the parabolic reflector. The heat flux values on the outer wall of the absorber were determined by multiplying the direct normal irradiation (I) by local concentration ratio (LCR) (q''_{wall}=I.LCR). Direct normal irradiance (I) was taken as I=1000 W/m^2. The LCR values for the commercial LS-2 parabolic trough solar collector is taken from Reference [6]. The curve was fitted to the LCR values and assigned to the absorber outer surface as a boundary condition by the user-defined function (UDF). In Figure 3a and 3b, LCR and the heat flux distribution on the outer wall of the absorber for the rim angle (θ_r) of θ_r=70º were given. In parabolic trough solar collectors, the outer surface of the absorber is surrounded by vacuumed cover glass. Therefore, conduction and convection heat losses from the absorber can be neglected. In this study, it was focused on the thermal performance and pressure losses. Therefore, the radiation heat transfer loss on the outer surface of the absorber was not taken into account as in the References [6] and [21].

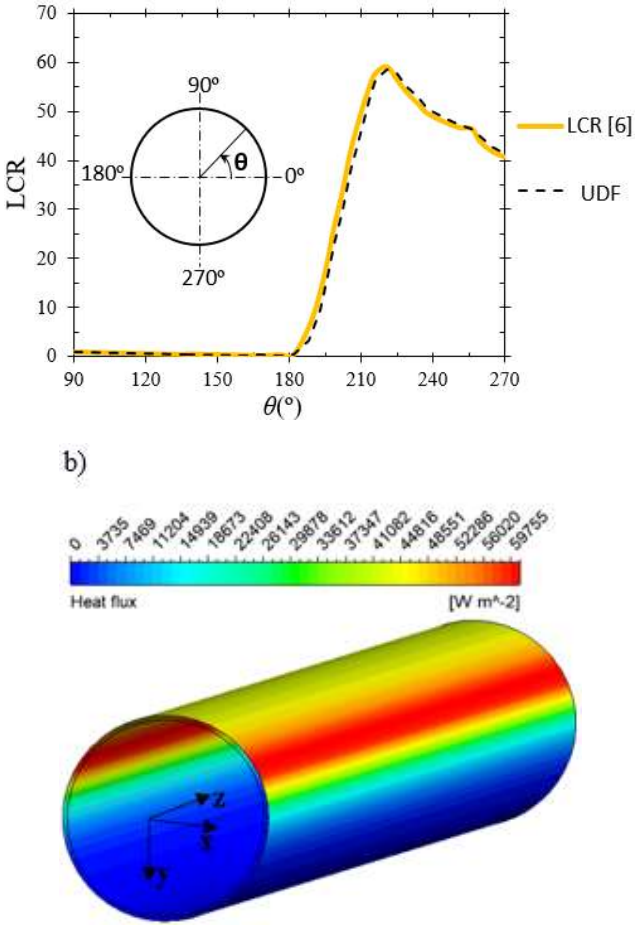

Figure 3. LCR and heat flux distribution on the outer wall of the absorber

Absorber inlet and outlet surfaces on the x-y plane were assumed to be adiabatic ($q'' = 0$). The no-slip boundary condition was defined on all solid surfaces in the fluid zone (u=0,v=0,w=0). In the y-z plane, the symmetry condition was applied such that the normal gradients of all flow variables were zero.

4. NUMERICAL METHOD

The Finite Volume Method was used to solve differential governing equations. It was utilized from ANSYS Fluent commercial package program to solve the analyzes. The SIMPLE algorithm was adopted for pressure and velocity coupling. The Second Order Upwind method was selected for the solution of discretized governing equations. Enhanced wall treatment [19] was applied in the flow analysis of the areas near the inner wall of the absorber. Residual value ($\varphi_{new} - \varphi_{old}$) was given by Equation 14 for the continuity equation, momentum equation, turbulent kinetic energy, turbulent dissipation rate, and energy equation.

$$|\varphi_{new} - \varphi_{old}| \leq 10^{-6} \quad (14)$$

Where, φ represents any variable.

5. REDUCTION OF NUMERICAL DATA

In the assessment of thermal performance, it was utilized from the dimensionless variables given below.

Reynolds number (Re) was determined by Equation15,

$$Re = \frac{w_{in} D_i}{\upsilon} \quad (15)$$

Where w_{in} is the fluid inlet velocity in the z-direction, υ is the kinematic viscosity of the fluid and D_i is the inner diameter of the absorber.

For the heat transfer analysis, the average Nu are given by the following equation,

$$Nu = h\frac{D_i}{\lambda} \quad (16)$$

In the equation, λ and h represent thermal conductivity of the fluid and convection heat transfer coefficient, respectively.

Heat transfer coefficient can be calculated by following equation,

$$h = \frac{q''}{(T_{wi} - T_b)} \quad (17)$$

Where T_{wi} is the average inner wall temperature of the absorber, T_b is the average fluid temperature and q'' is the average heat flux on the receiver wall.

Friction coefficient (f) was calculated with Equation 18,

$$f = \frac{\Delta P(D_i/L)}{\rho {w_{in}}^2/2} \quad (18)$$

Where, ΔP and f are the pressure loss and friction coefficient, respectively

Petukhov and Gnielinski correlations [17] were used for f and Nu, respectively for the validation of pipe flow. Gnielinski correlation is valid in the range of $3x10^3 \leq Re \leq 5x10^6$.

Petukhov correlation:

$$f = (0.790 lnRe - 1.64)^{-2} \quad (19)$$

Gnielinski correlation:

$$Nu = \frac{\left(\frac{f}{8}\right)(Re-1000)Pr}{1+12.7\left(\frac{f}{8}\right)^{\frac{1}{2}}\left(Pr^{\frac{2}{3}}-1\right)} \quad (20)$$

Equation 21 [21] was used to compare thermal performance between different conditions for identical pumping power,

$$\psi = (Nu_{800}/Nu)/(f_{800}/f)^{1/3} \quad (21)$$

Where, Nu_{800} and f_{800} denote the Nusselt number and friction coefficient for the Syltherm 800 oil in any condition. Nu and f are Nusselt number and friction coefficient values which are formed according to other thermal oil types. The non-uniform heat flux distribution on the absorber outer surface increases the circumferential temperature difference on the absorber. This leads to the formation of bending stresses and damage to the vacuumed glass cover [23,24]. With the following equation, the maximum circumferential temperature difference ratios (Γ) on the absorber were determined.

$$\Gamma = \frac{\Delta T_{max}}{\Delta T_{max,800}} \quad (22)$$

Where, $\Delta T_{max,800}$ is the maximum circumferential temperature difference for Syltherm 800 oil, ΔT_{max} is used for other thermal oil types. ΔT_{max} was calculated by Equation 24,

$$\Delta T_{max} = T_{max,o} - T_{min,o} \quad (24)$$

Where, $T_{max,o}$ and $T_{min,o}$ represent the maximum and minimum outer surface average temperature of the absorber.

6. VALIDATION OF NUMERICAL RESULTS

To verify the numerical results, the grid size independence test was performed first. Table 2 shows a grid size comparison for the case without fin and the case with flat fin. For both conditions, the deviation in the values of the variables is approximately 1% for the grid dimensions below 2.5 mm. Thus, 2.5 mm grid size was selected for numerical analysis.

Table 3. Grid size independence test reults (Re=4x10^4, T_{in}=300K, Syltherm 800 oil)

Grid size	*f*	Deviation(%)	*Nu*	Deviation(%)
Absorber without fin				
6mm	0.02269	-	809.75	-
4mm	0.02266	0.110743	794.37	1.89873
2.5mm	0.02288	0.957665	776	2.31338
1.25mm	0.02296	0.335939	770	0.77196
Absorber with flat fin				
6mm	0.01925	-	1104.45	-
4mm	0.01850	3.886995	1162.58	5.26315
2.5mm	0.01831	1.033374	1039.48	10.58823
1.25mm	0.01831	0.021484	1027.395	1.16279

The grid structure for the 2,5 mm grid size was shown in Figure 4. The unstructured grid was used in the fluid zone and the grid structure was concentrated in areas close to the solid surfaces. For the absorber tube, however, structured grid was used with uniform distribution. For the grid density on solid surfaces, the y^+ value is approximately $y^+ = 1$ for all analyzes. y^+ is expressed by Equation 25,

$$y^+ = \sqrt{yu_t/v} \quad (25)$$

Where, *y* represents the distance from the solid surface, v represents the kinematic viscosity, and u_t represents the friction velocity. u_t is determined by following equation,

$$u_t = \sqrt{\tau_w/\rho} \quad (26)$$

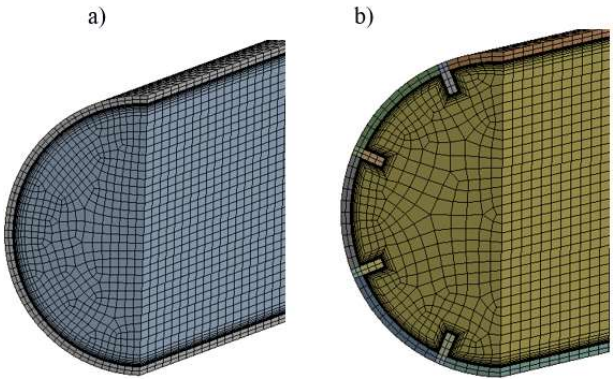

Figure 4. Grid structure a) without fin, b) flat/sinusoidal fin

The comparison of *f* and *Nu* values with literature studies was carried out for the case with and without fin. The results of *f* and *Nu* were compared with Petukhov and Gnielinski correlations, respectively. In literature studies, it was stated that 20% error was acceptable in industrial applications for these correlations [3,21]. In addition, these correlations are affected at negligible level from the heat flux distribution outside the absorber [17]. Figures 5a and 5b show comparisons of *Nu* and *f* for the case without fin. For *Nu* and *f*, the highest deviation was observed 8% and 10% respectively.

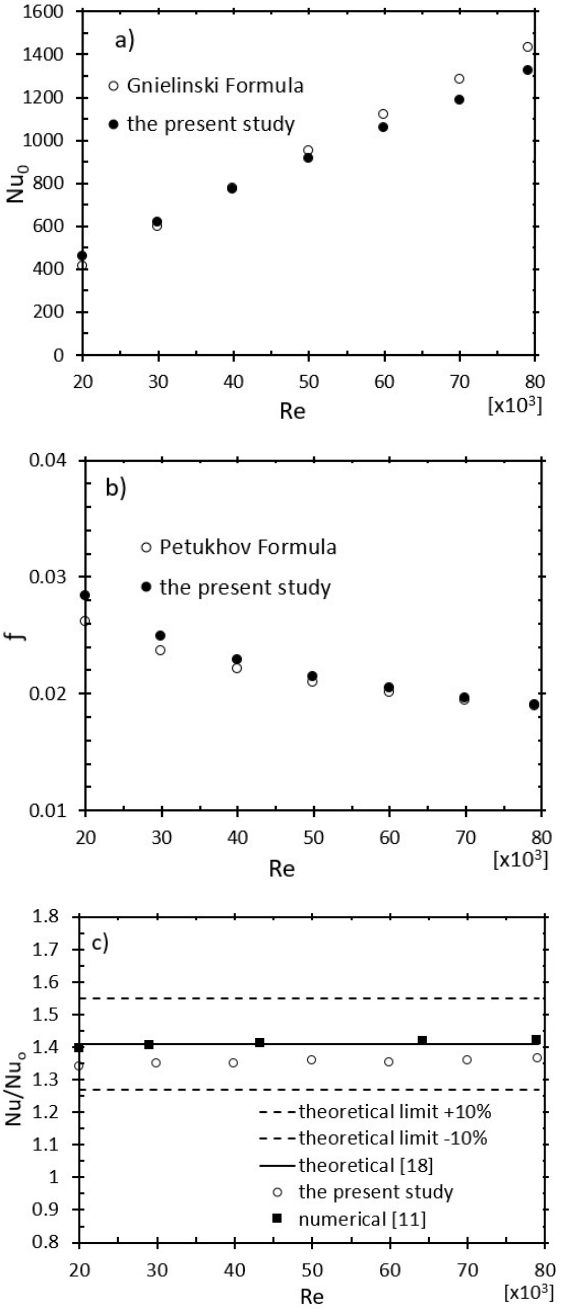

Figure 5. Validation of numerical results a) *Nu*, without fin, b) *f*, without fin, c) Nu/Nu_{flat} ratio

The results of the theoretical and numerical study in the literature have been used for the validation of flat fin condition (Figure 5c). The *Nu* ratios in the cases with and without fin were given in Figure 5c. The deviation between the results in this study and the literature studies was found to be around 4%. These findings indicate that the applied mathematical model and numerical analysis are in good agreement with the results of the literature studies.

7. RESULTS AND DISCUSSIONS

Numerical analyzes were carried out for turbulent flow conditions in the range of $Re=2x10^4$-$8x10^4$.The results were presented below as graphs containing velocity vectors, temperature contours, circumferential temperature difference and thermal enhancement factor.

7.1. Velocity and Temperature Distribution

In the study, it was aimed to increase the convection around the fin with sinusoidal lateral surface structure in the absorber. In addition, the interaction of different thermal oils types with fin geometries was investigated. In Figure 6b, velocity vectors formed in flat and sinusoidal fin structure were given. As shown in Figure 6, the sinusoidal lateral structure of the fin caused the fluid to change direction. Thus, it was provided increase in convection. Figure 7 shows the velocity vectors formed by the use of sinusoidal fins for different types of thermal oil. Due to the different thermophysical properties of the thermal oils, different fluid velocities occurred in the absorber for the certain Re value. It was observed that the highest and lowest fluid velocity values were formed for Sylthern 800 and Therminol D12 thermal oils, respectively. The increase in fluid velocity also increased the convection around the fin.

The effect of the fin geometry and fluid type on the temperature distribution can be examined with Figures 8 and 9. Figure 8 shows the effect of the use of the internal longitudinal fin on the fluid temperature. As seen in Fig. 8a, a non-uniform temperature distribution occurred in the case without fin and this increased the temperature difference in the absorber depending on the heat flux density. With the use of the fins, the heat transfer surface area increased and the absorber temperatures decreased (Figures 8b and 8c). Furthermore, with the sinusoidal fin surface, fluid motion increased and a more uniform temperature distribution was obtained (Figure 8c).

The effects of different thermal oil types on the temperature distribution for the sinusoidal fin type was given in Figure 9. The lowest absorber temperature and the most uniform temperature distribution were obtained for Sylthern 800 thermal oil (Figure 9c). On the other hand, the lowest heat transfer was observed for Therminol D12 thermal oil type.

a)

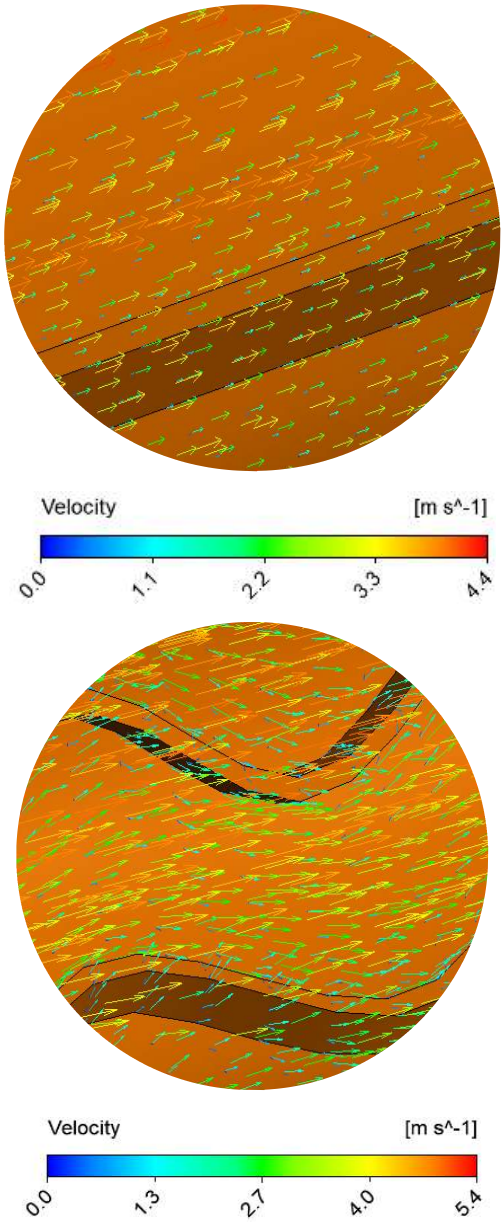

Figure 6. Velocity vectors (Re=60000, Sylthern 800 oil) a) flat fin, b) sinusoidal fin

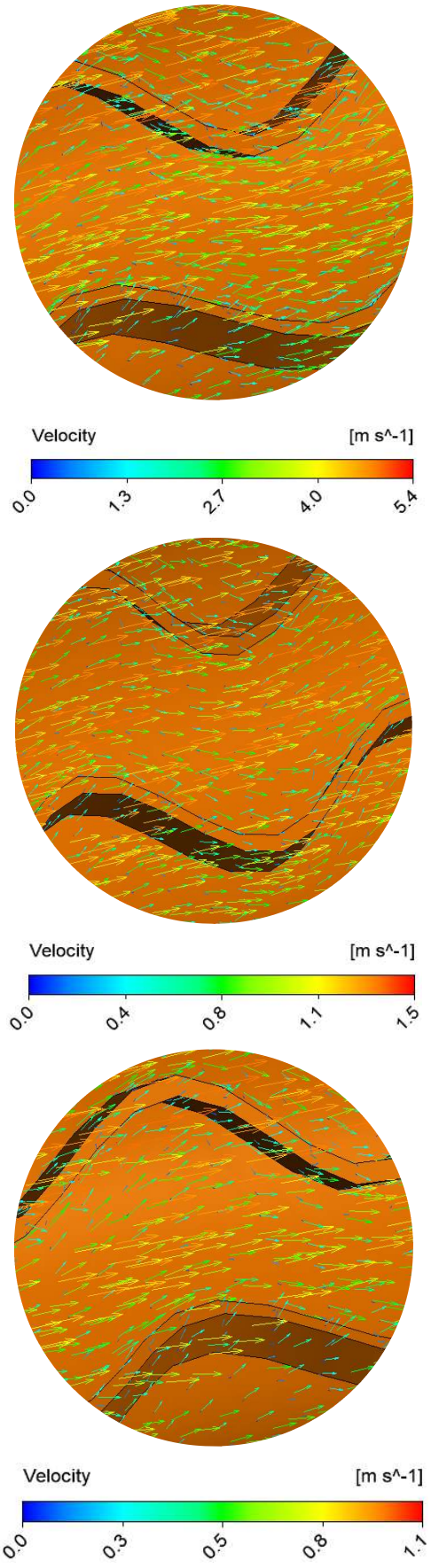

Figure 7. Velocity vectors (Re=60000, Sinusoidal fin) a) Syltherm 800, b) Therminol VP1, c) Therminol D12

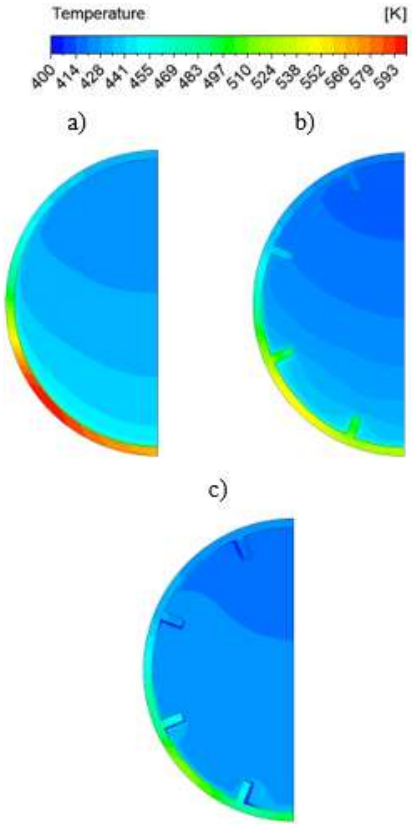

Figure 8. Temperature contours (Re=20000, Therminol VP1) a) without fin, b)flat fin, c) sinusoidal fin

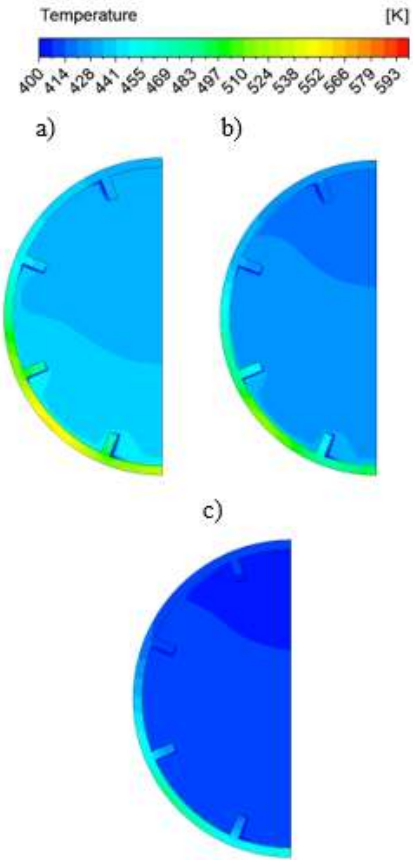

Figure 9. Temperature contours (Re=20000, sinusoidal fins) a) Therminol D12, b) Therminol VP1, c) Syltherm 800

Figure 10 shows the temperature distributions of the fluid and absorber depending on the absorber length in the use of different types of oil for the sinusoidal fin type. For all oil types, heat transfer was obtained the highest in the fluid inlet zone and lowest in the outlet zone. Therefore, the absorber temperature began to increase towards the absorber outlet. In the fluid zone, the oil temperature increased with the effect of convection towards the absorber outlet. The highest convection around the fin was occurred for the Syltherm800 oil and the lowest absorber temperatures were obtained.

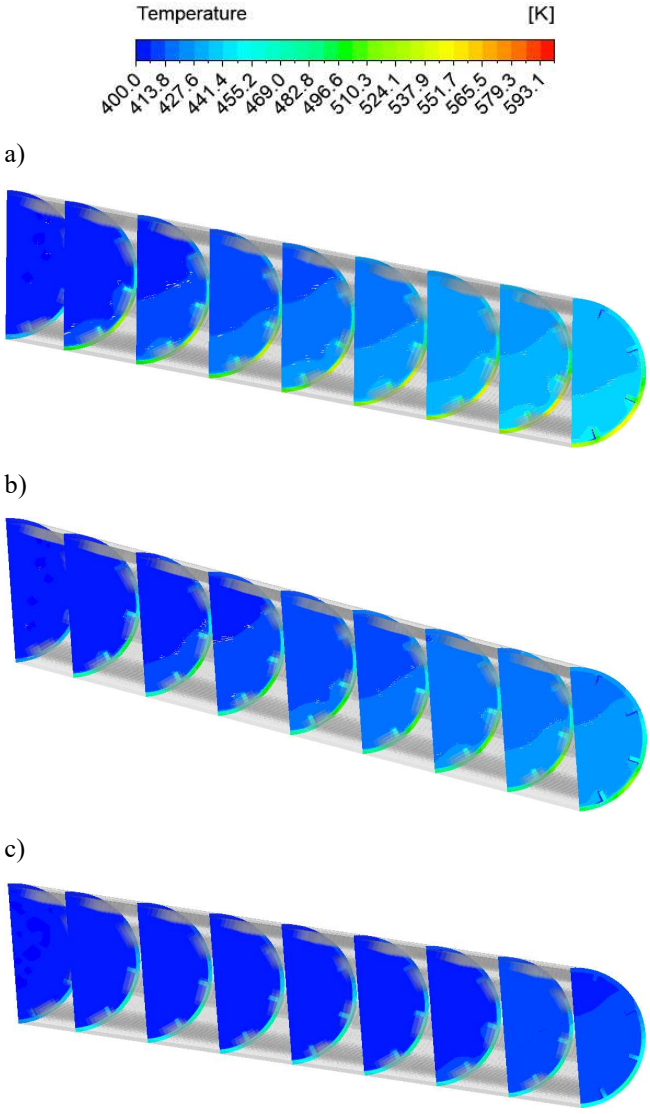

Figure 10. Temperature variations with absorber length (Re=20000, sinusoidal fins) a) Therminol D12, b) Therminol VP1, c) Syltherm 800

7.2. Thermal Performance Analysis

Thermal performance evaluation of thermal oil types was made with reference to Syltherm 800 thermal oil for all conditions with and without fin usage (Figure 11a). Figure 11a shows the thermal performance curves of the Therminol D12 and VP1 type thermal oils with respect to the Syltherm 800 type thermal oil at variable Re values for an identical pumping power. With the increase in the Re, the heat transfer in the use of Syltherm 800 oil for the cases with flat fin and without fin increased with respect to the heat transfer in the Therminol D12 and VP1 oil use. The highest thermal enhancement factor was achieved in the use of fin with sinusoidal lateral surface, and the heat transfer ratio between the oils remained nearly constant in all the Re values. With the use of Syltherm 800 oil, the thermal enhancement factor increased by 1.4 and 1.44 times respectively according to the Therminol VP1 and D12 oil type for the case with sinusoidal fin. This revealed that the highest and lowest thermal performance occurred for Syltherm 800 and Therminol D12 type thermal oils, respectively.

Figure 11b indicates the ratios of the maximum circumferential temperature differences on the absorber outer surface for different oil types. With the increase in the Re and the use of sinusoidal fin, the temperature difference ratios decreased. When oil types were compared, it was observed that the highest absorber temperatures occurred in Therminol D12 oil usage. For the Therminol D12 oil usage, the maximum circumferential temperature difference ratio increased in the range of 1.73-1.90 according to the use of Syltherm 800 oil.

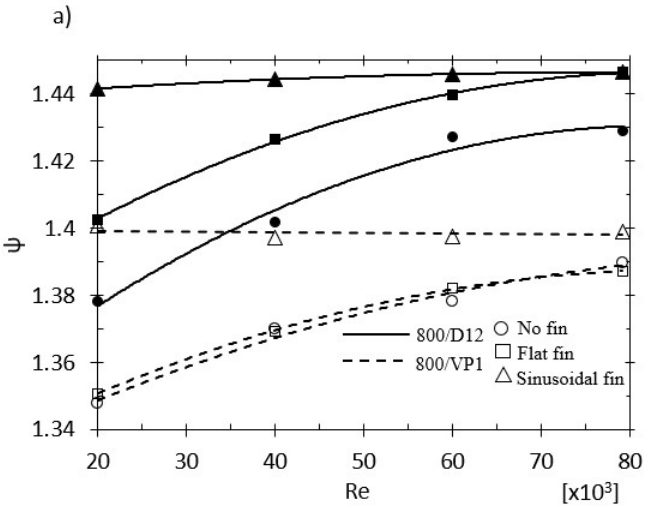

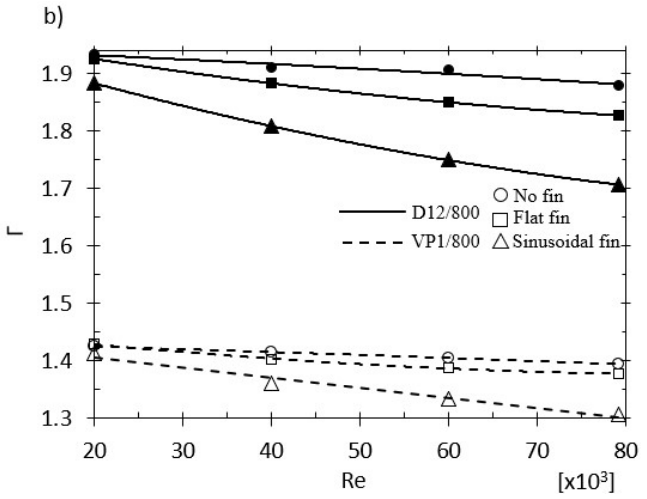

Figure 11. Comparison of thermal oils a) Thermal enhancement factor, b) Maximum circumferential temperature difference ratio

8. CONCLUSIONS

In a parabolic trough solar collector, the analysis of the internal longitudinal fin use with different geometries for different types of thermal oil was carried out and the results obtained were summarized below.

The use of the internal fin with sinusoidal lateral surface for all types of thermal oil increased the convection by directing the fluid. This situation increased the heat transfer to the fluid compared to the flat fin and finless conditions and decreased the absorber temperature. Furthermore, the sinusoidal fin made the temperature distribution in the fluid more uniform.

The highest thermal enhancement factor was obtained for Syltherm 800 oil. With the use of Syltherm 800 oil, the thermal enhancement factor increased by 40% and 44% respectively according to the Therminol VP1 and D12 oil type for the case with sinusoidal fin. Parallel to the results of thermal performance, the highest absorber temperatures occurred in the use of Therminol D12 oil. For the Therminol D12 oil usage, the maximum circumferential temperature difference ratio increased in the range of 73-90% according to the use of Syltherm 800 oil.

REFERENCES

[1] W. Fuqiang, T. Zhexiang, G. Xiangtao, T. Jianyu, H. Huaizhi and L. Bingxi, "Heat transfer performance enhancement and thermal strain restrain of tube receiver for parabolic trough solar collector by using asymmetric outward convex corrugated tube," *Energy,* vol. 114, pp. 275-292, 2016.

[2] W. Fuqiang, C. Ziming, T. Jianyu, Y. Yuan, S. Yong and L. Linhua, "Progress in concentrated solar power technology with parabolic trough collector system: A comprehensive review," *Renewable and Sustainable Energy Reviews*, vol. 79, pp. 1314-1328, 2017.

[3] Z. D. Cheng, Y. L. He and F. Q. Cui, "Numerical study of heat transfer enhancement by unilateral longitudinal vortex generators inside parabolic trough solar receivers," *International journal of heat and mass transfer*, vol. 55, no. 21-22, pp. 5631-5641, 2012.

[4] D. R. Waghole, R. M. Warkhedkar and R. K. Shrivastva, "Experimental investigations on heat transfer and friction factor of silver nanofluid in absorber/receiver of parabolic trough collector with twisted tape inserts," *Energy Procedia*, vol. 45, pp. 558-567, 2014.

[5] K. R. Kumar and K. S. Reddy, "Effect of porous disc receiver configurations on performance of solar parabolic trough concentrator," *Heat and Mass Transfer*, vol. 48, no. 3, pp. 555-571, 2012.

[6] P. Wang, D. Y. Liu and C. Xu, "Numerical study of heat transfer enhancement in the receiver tube of direct steam generation with parabolic trough by inserting metal foams," *Applied energy*, vol. 102, pp. 449-460, 2013.

[7] S. Ghadirijafarbeigloo, A. H. Zamzamian and M. Yaghoubi, "3-D numerical simulation of heat transfer and turbulent flow in a receiver tube of solar parabolic trough concentrator with louvered twisted-tape inserts," *Energy procedia*, vol. 49, pp. 373-380, 2014.

[8] O. A. Jaramillo, M. Borunda, K. M. Velazquez-Lucho and M. Robles,"Parabolic trough solar collector for low enthalpy processes: An analysis of the efficiency enhancement by using twisted tape inserts," *Renewable Energy,* vol. 93, pp. 125-141, 2016.

[9] Z. Huang, G. L. Yu, Z. Y. Li and W. Q. Tao, "Numerical study on heat transfer enhancement in a receiver tube of parabolic trough solar collector with dimples, protrusions and helical

fins," *Energy Procedia*, vol. 69, pp. 1306-1316, 2015.

[10] X. Gong, F. Wang, H. Wang, J. Tan, Q. Lai and H. Han, "Heat transfer enhancement analysis of tube receiver for parabolic trough solar collector with pin fin arrays inserting," Solar *Energy*, vol. 144, pp. 185-202, 2017.

[11] E. Bellos, C. Tzivanidis and D. Tsimpoukis, "Thermal enhancement of parabolic trough collector with internally finned absorbers," *Solar Energy,* vol. 157, pp. 514-531, 2017.

[12] Y. Demagh, I. Bordja, Y. Kabar and H. Benmoussa, "A design method of an S-curved parabolic trough collector absorber with a three-dimensional heat flux density distribution," *Solar Energy,* vol. 122, pp. 873-884, 2015.

[13] N. R. Rosaguti, D. F. Fletcher and B. S. Haynes, "Low-Reynolds number heat transfer enhancement in sinusoidal channels," *Chemical engineering science,* vol. 62, no. 3, pp. 694-702, 2007.

[14] Y. Sui, C. J. Teo and P. S. Lee, "Direct numerical simulation of fluid flow and heat transfer in periodic wavy channels with rectangular cross-sections," *International Journal of Heat and Mass Transfer,* vol. 55, no. 1-3, pp. 73-88, 2012.

[15] A. Fernández-García, E. Zarza, L. Valenzuela, and M. Pérez, "Parabolic-trough solar collectors and their applications," *Renewable and Sustainable Energy Reviews,* vol. 14, no. 7, pp. 1695-1721, 2010.

[16] R. Forristall, "Heat transfer analysis and modeling of a parabolic trough solar receiver implemented in engineering equation solver (No. NREL/TP-550-34169)," *National Renewable Energy Lab.,* Golden, CO.(US), 2003.

[17] Y. A. Cengel, and A. J. Ghajar, "Heat and mass transfer (a practical approach, SI version).", 2011.

[18] M. K. Jensen and A. Vlakancic, "Technical Note Experimental investigation of turbulent heat transfer and fluid flow in internally finned tubes," *International Journal of Heat and Mass Transfer,* vol. 42, no. 7, pp. 1343-1351, 1999.

[19] Ansys Inc., "ANSYS FLUENT 14.0 Theory Guide," 2011.

[20] H. K. Versteeg and W. Malalasekera, "An introduction to computational fluid dynamics: the finite volume method," Pearson Education, 2007.

[21] Z. Huang, Z. Y. Li, G. L. Yu and W. Q. Tao, "Numerical investigations on fully-developed mixed turbulent convection in dimpled parabolic trough receiver tubes," *Applied Thermal Engineering,* vol. 114, pp.1287-1299, 2017.

[22] R. L. Webb, "Performance evaluation criteria for use of enhanced heat transfer surfaces in heat exchanger design," *International Journal of Heat and Mass Transfer,* vol. 24, no. 4, pp. 715-726, 1981.

[23] S. Khanna, S. B. Kedare and S. Singh, "Deflection and stresses in absorber tube of solar parabolic trough due to circumferential and axial flux variations on absorber tube supported at multiple points," *Solar Energy*, vol. 99, pp. 134-151, 2014.

[24] S. Khanna, V. Sharma, S. B. Kedare and S. Singh, "Experimental investigation of the bending of absorber tube of solar parabolic trough concentrator and comparison with analytical results," *Solar Energy,* vol. 125, pp. 1-11, 2016.

[25] Eastman Therminol® heat transfer fluids, https://www.therminol.com (Accessed 2018-12-7).